ACS OMEGA

http://pubs.acs.org/journal/acsodf

Article

Cu/PCN Metal-Semiconductor Heterojunction by Thermal Reduction for Photoreaction of CO_2-Aerated H_2O to CH_3OH and C_2H_5OH

Huihui Du, Xinhua Gao, Qingxiang Ma, Xiaojiao Yang, and Tian-Sheng Zhao*

Cite This: *ACS Omega* 2022, 7, 16817−16826

Read Online

ACCESS | Metrics & More | Article Recommendations | Supporting Information

ABSTRACT: g-C_3N_4-based materials show potential for photoreduction of CO_2 to oxygenates but are subjected to fast recombination of photogenerated charge carriers. Here, a novel Cu-dispersive protonated g-C_3N_4 (PCN) metal-semiconductor (m-s) heterojunction from thermal reduction of a Cu_2O/PCN precursor was prepared and characterized using in situ X-ray diffraction, scanning transmission electron microscopy, X-ray photoelectron spectroscopy, ultraviolet−visible (UV−vis) spectra, photoluminescence (PL) spectra, transient photocurrent response, and electrochemical impedance spectroscopy (EIS). The Cu amount in Cu/PCN and the reduction temperature affected the generation of CH_3OH and C_2H_5OH from the photoreaction of CO_2-aerated H_2O. During calcination of Cu_2O/PCN in N_2 at 550 °C, Cu_2O was completely reduced to Cu with even dispersion, and a m-s heterojunction was obtained. With thermal exfoliation, Cu/PCN showed a specific surface area and layer spacing larger than those of PCN. Cu/PCN-0.5 (12.8 wt % Cu) exhibited a total carbon yield of 25.0 μmol·g^{-1} under UV−vis irradiation for 4 h, higher than that of Cu_2O/PCN (13.6 μmol·g^{-1}) and PCN (6.0 μmol·g^{-1}). The selectivity for CH_3OH and C_2H_5OH was 51.42 and 46.14%, respectively. The PL spectra, transient photocurrent response, and EIS characterizations indicated that Cu/PCN heterojunction promotes the separation of electrons and holes and suppresses their recombination. The calculated conduction band position was more negative, which is conducive to the multielectron reactions for CH_3OH and C_2H_5OH generation.

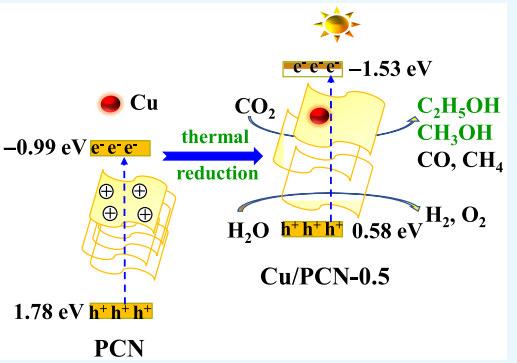

INTRODUCTION

Light-energy-boosted transformation of CO_2 and H_2O into oxygenates as well as hydrocarbons is desired for sustainable energy exploration of our planet. Semiconductor materials such as TiO_2,[1] ZnO,[2] $BiVO_4$,[3] ZnV_2O_4,[4] g-C_3N_4,[5] or Cu_2O[6] have been studied for methanol generation from the photoreaction of CO_2 and H_2O. Easily available g-C_3N_4-based materials have attracted interest due to their unique 2D-layered structure and narrow band gap (~2.7 eV) that respond to visible light energy absorption.[7] However, fast recombination of light-excited charge carriers on g-C_3N_4 is adverse to the photoassisted actions.[8] Methods to extend the duration time of photogenerated carriers include exfoliation, metal modification, or semiconductor combination.[9] A Au, Ag, or Pd composite g-C_3N_4 enhanced electron transfer and photoreaction,[10−12] although these metals are expensive.

Earth-abundant copper has received attention for photoreduction of CO_2 owing to its photocatalytic performance and potential in the formation of C_{2+} products,[13,14] with Cu^{2+}, Cu^+, and Cu^0 for CO_2 adsorption, photoreduction reaction, and charge separation, respectively. Cu_2O-decorated g-C_3N_4 dominated CO production in the gas-phase photoconversion of CO_2 through a H_2O bubbler due to interfacial charge transfer.[15] Cu_2O/polymeric carbon nitride assisted CO_2 in water to methanol owing to high redox potentials (E_{CB} = −1.15 eV, E_{VB} = 1.65 eV), *Z*-schematic charge flow, and spatial separation of electrons and holes.[16] A g-C_3N_4-encapsulated Cu_2O nanowire as a *Z*-scheme heterojunction showed enhanced methanol yield and selectivity from the gas-phase photoreaction of CO_2 with H_2O by facilitating rapid separation of photogenerated electrons and holes.[17] Furthermore, under illumination on the (110) face of rhombic dodecahedral Cu_2O, Cu^+ was converted to Cu^{2+} with coadsorption of CO_2 and H_2O,[18] demonstrating the active site action of Cu^+. The synergistic effect of Cu^0 and Cu^+ on CO_2 reduction was reported for Cu/Cu^+@TiO_2,[1] as Cu^+ accelerates charge carrier transfer, whereas Cu acts as the active site for CO_2 reduction or as an electron reservoir. AuCu alloy modified ultrathin and porous g-C_3N_4 nanosheets with strong interaction between metal and g-C_3N_4 accelerated the migration of photogenerated charges, and the Cu surface promoted the intermediates $CO_2^{\bullet-}$ and *CO for photothermal conversion of CO_2 to ethanol.[19]

Received: March 25, 2022
Accepted: April 18, 2022
Published: May 2, 2022

https://doi.org/10.1021/acsomega.2c01827
ACS Omega 2022, 7, 16817−16826

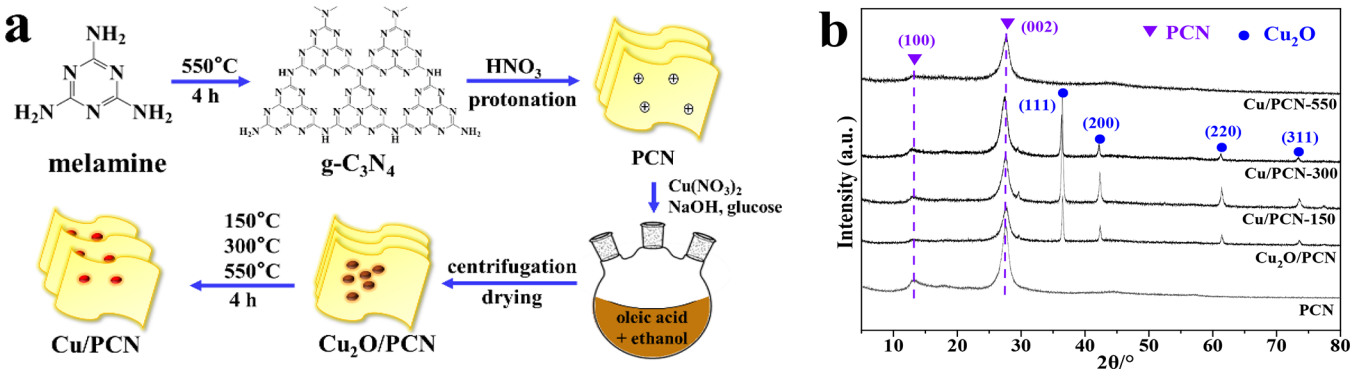

Figure 1. (a) Preparation procedure for Cu/PCN and (b) XRD patterns of Cu/PCN-*x*, where *x* is the calcination temperature.

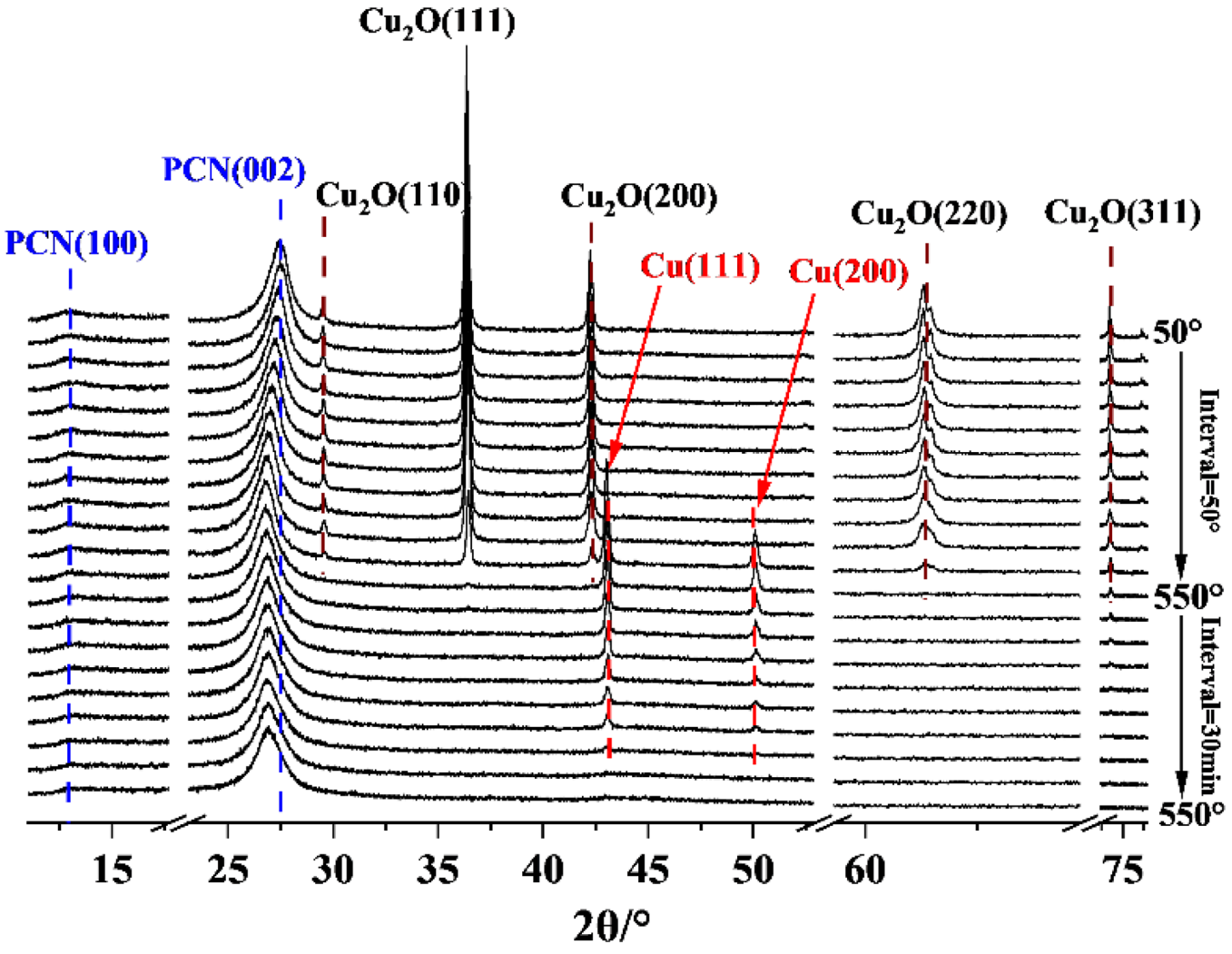

Figure 2. In situ XRD patterns of the Cu_2O/PCN-0.5 precursor.

Composite Cu/ZnO/g-C_3N_4 enhanced methanol generation from CO_2 and H_2O due to suppression of recombination.[2] Cu-based electrocatalyst studies indicated that CO_2 reduction inclines to multicarbon products (C_2^+) on Cu^+ sites.[20,21] This progress reveals distinct impacts of the Cu valence in semiconductor materials on the photoreaction products.

Solution reduction was used for atomically dispersed Cu on ultrathin TiO_2 nanosheets.[22] However, the process is tedious. In situ synthesized Cu/Cu_2O using calcination displays a response extension from visible light to the near-IR region associated with excitation of Cu-localized surface plasmon resonance.[23] Mott−Schottky-type nanohybrids (Cu/NC) with 750 °C condensation increased the Schottky barrier of the Cu−C for CO_2 fixation.[24]

For the above-mentioned process, it is possible that Cu/g-C_3N_4 can be obtained through a thermal reduction method and photoreduction of CO_2 to C_{2+} products besides methanol.[25]

In this work, g-C_3N_4 and Cu_2O were prepared using thermal polymerization and a solution method, respectively, and the

https://doi.org/10.1021/acsomega.2c01827
ACS Omega 2022, 7, 16817−16826

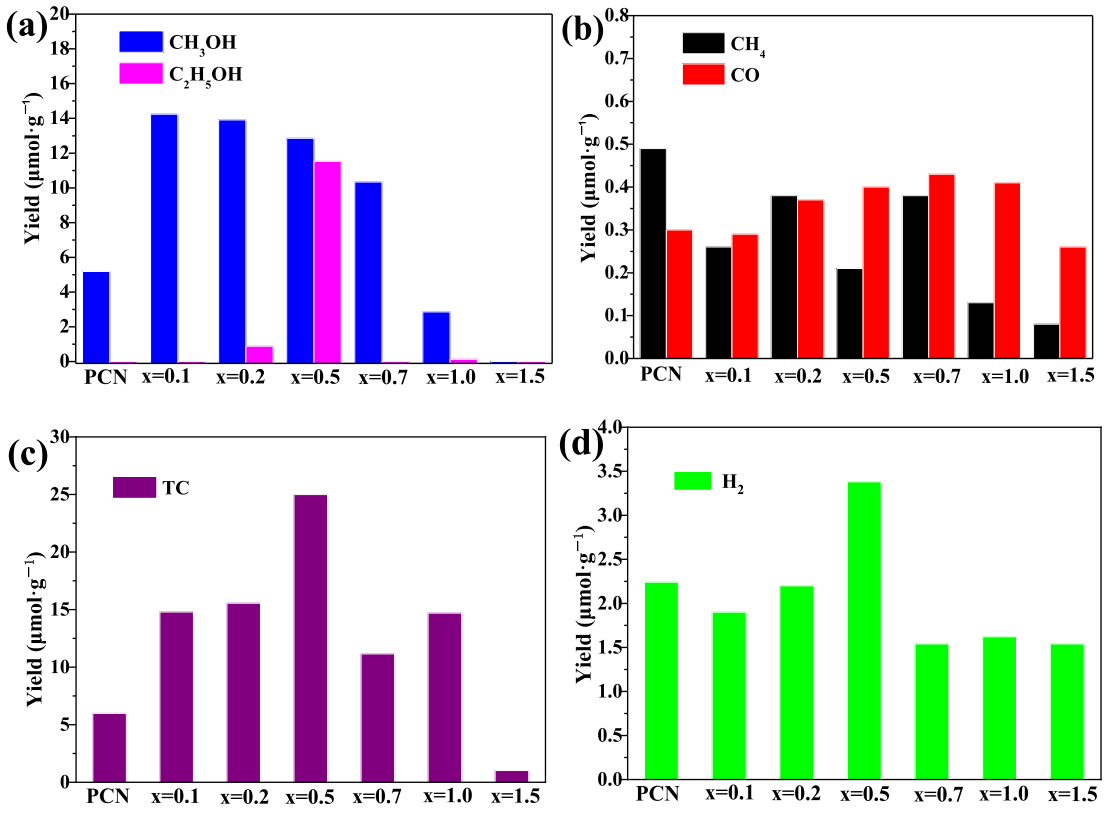

Figure 3. Reaction activity of CO_2-aerated H_2O on Cu/PCN-*x*. Yields for (a) CH_3OH and C_2H_5OH, (b) CH_4 and CO, (c) total carbon, and (d) H_2. Conditions: 40 mg of catalyst, 80 °C, 0.2 MPa, UV−vis irradiation 4 h.

Cu/PCN m-s heterojunction was obtained using thermal reduction. The resulting Cu/PCN exhibited higher yields toward alcohols. The CH_3OH and C_2H_5OH generation were promoted by a multielectron reaction due to strong interaction on the Cu/PCN m-s heterojunction and a remarkable change in energy level positions, as proven by structural characterizations.

RESULTS AND DISCUSSION

Phases of Synthesized Samples. From Cu_2O/PCN (protonated g-C_3N_4) precursor and using the thermal reduction process in a N_2 atmosphere, the Cu-dispersive PCN (Cu/PCN) was obtained as depicted in Figure1a. Cu/PCN-0.5 (12.8 wt % Cu) samples showed X-ray diffraction (XRD) peaks at 2θ of 12.8 and 27.6° (Figure1b), ascribed to the (100) and (002) crystal planes of g-C_3N_4 (Figure 4).[26] The diffraction peaks at 2θ of 36.4, 42.3, 61.3, and 73.5° are ascribed to the (111), (200), (220), and (311) crystal planes of Cu_2O (PDF# 05-0667). As the reduction temperature for Cu_2O/PCN-0.5 was increased from 150 to 300 °C, the peak intensity of Cu_2O decreased. After undergoing 550 °C calcination for 4 h, these peaks disappeared. It was inferred that Cu_2O is reduced to Cu by the reductive PCN, and the resulting Cu species are well-dispersed even in the monolayer.

When the nominal Cu amount was greater than 32% (Table S1, calcination temperature 550 °C), the peaks at 2θ of 43.3, 50.4, and 74.1° corresponding to the (111), (200), and (220) crystal planes of Cu were observed (Figure S1), indicating low dispersion of a high Cu composite.

To identify the Cu species, the thermal reduction process of the Cu_2O/PCN-0.5 precursor was traced using in situ XRD, and the results are shown in Figure 2. As the temperature was increased from 50 to 550 °C in N_2 flow, the diffraction patterns were recorded in a temperature interval of 50 °C and in an interval of 30 min when the temperature was kept constant at 550 °C for 4 h. The two diffraction peaks of PCN were observed, indicating that introduction of Cu and calcination temperature do not affect the PCN phase. The shifting of the diffraction peak at 2θ of 27.6° demonstrated the increased layer spacing of PCN associated with thermal exfoliation.[9] Below 550 °C, the diffraction peak intensity of Cu_2O gradually diminished until it disappeared. Starting from 450 °C, the diffraction peaks of Cu appeared and the intensity increased gradually with the increase in temperature. The diffraction peaks corresponding to the Cu(111) and Cu(200) planes slightly shifted to 2θ of 43.0 and 50.1° owing to the existence of a mixed phase[19,23] like Cu_2O−Cu. During the constant temperature of 550 °C for 240 min, the diffraction peaks of Cu gradually shrank until they disappeared completely, demonstrating that, on the one hand, Cu_2O is completely reduced to Cu. On the other hand, the resulting Cu is evenly dispersed in the monolayer on PCN. It should be noted that the Cu^+ and Cu can be tuned with varying calcination temperature and time.

Photoreaction Activity. The photoreaction activity of CO_2-aerated H_2O on synthesized samples is shown in Figure 3. The products included CH_3OH, C_2H_5OH, CH_4, CO, and O_2 (O_2 not quantified considering possible reactions with the hole scavenger). From Figure 3a, the Cu amount in Cu/PCN significantly affected the yields of CH_3OH and C_2H_5OH. For Cu/PCN-0.1 with a high Cu amount, the main product was CH_3OH. Cu/PCN-0.2 and Cu/PCN-0.5 showed increased C_2H_5OH product, in particular, with about half−half CH_3OH−C_2H_5OH for Cu/PCN-0.5. From Cu/PCN-0.7 to

https://doi.org/10.1021/acsomega.2c01827
ACS Omega 2022, 7, 16817−16826

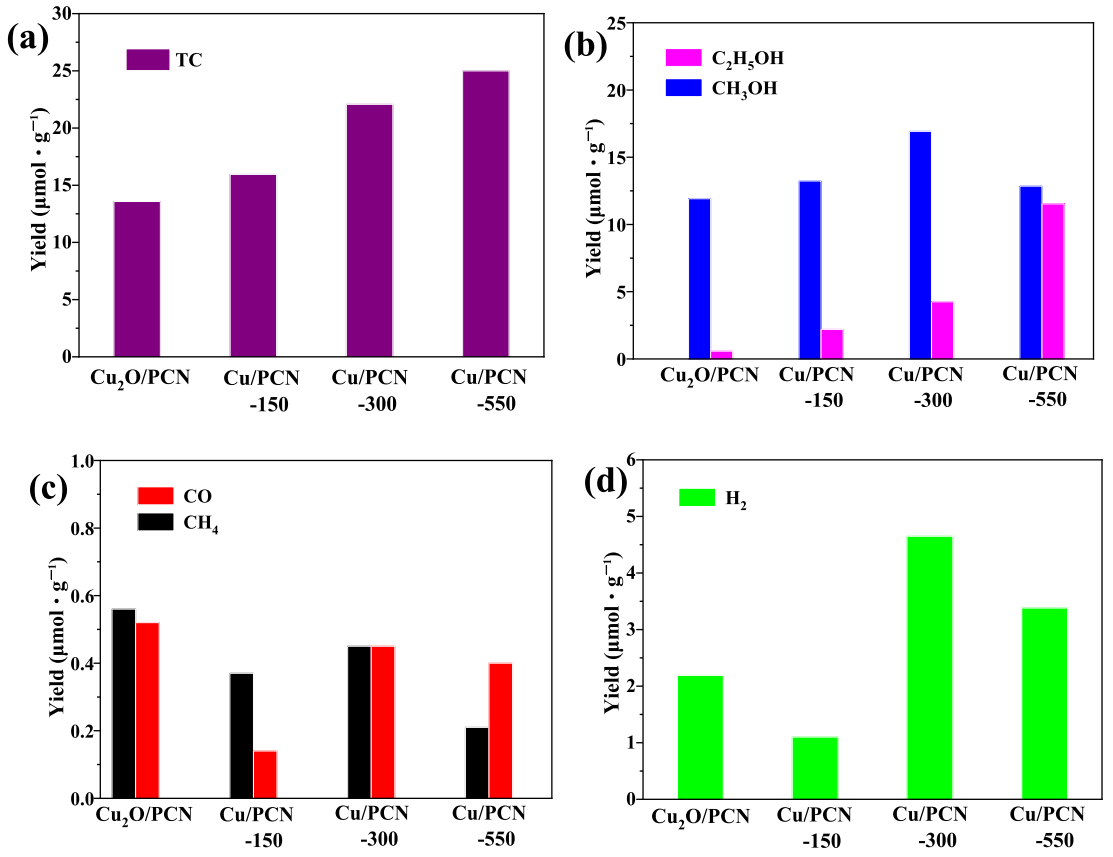

Figure 4. Activity of Cu/PCN-0.5 at different reduction temperatures. Yields for (a) total carbon, (b) CH_3OH and C_2H_5OH, (c) CH_4 and CO, and (d) H_2. Conditions: 40 mg of catalyst, 80 °C, 0.2 MPa, UV−vis irradiation 4 h.

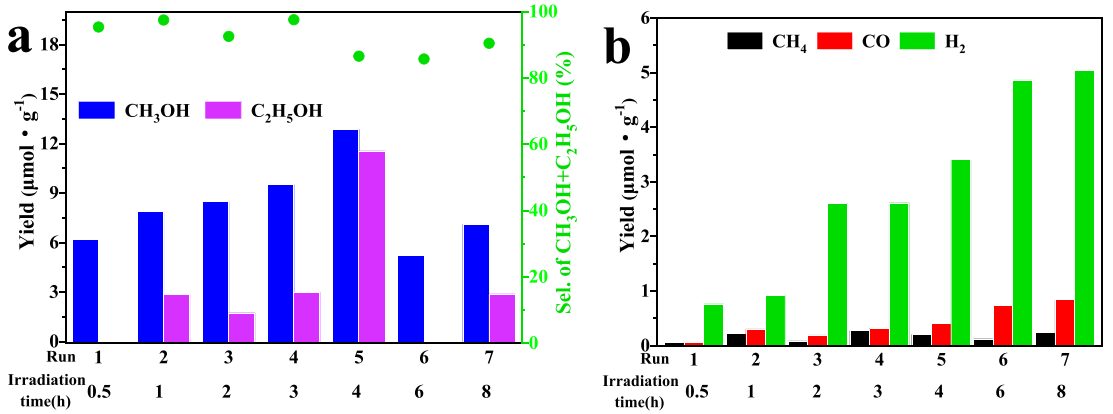

Figure 5. Effect of irradiation reaction time on activity. Yields for (a) CH_3OH and C_2H_5OH and (b) CH_4, CO, and H_2. Conditions: 40 mg of Cu/PCN-0.5, 80 °C, 0.2 MPa.

Cu/PCN-1.5, as the Cu amount decreased, the CH_3OH yield decreased. As the Cu amount varied (Figure 3b), the CH_4 and CO yields did not show evident change, considering the analysis error in low content. Cu/PCN-1.5 displayed the lowest yields of CO and CH_4 (even less than those on PCN) due to faster recombination of photogenerated carriers (Figure S2). Among all tests on the samples with different Cu amounts, the highest total carbon (TC) yield (25.0 μmol·g^{-1}) was achieved on Cu/PCN-0.5 (Figure 3c), 4.2 times higher than that on PCN, and the H_2 yield reached a maximum (Figure 3d). It was inferred that the promoted TC activity and CH_3OH and C_2H_5OH yields on the Cu-dispersive PCN are associated with the electron reservoir of Cu and Cu active sites.[1] However, there exists an appropriate amount of Cu. Under this circumstance, more photogenerated electron−holes on Cu/PCN might take place in the redox reactions of CO_2-aerated H_2O.

The photoreaction activity of CO_2-aerated H_2O on Cu/PCN-0.5 from different reduction temperatures is shown in Figure 4. As the temperature was increased from 150 to 550 °C, the TC yield for all carbon-containing products increased (Figure 4a). The TC yield of Cu/PCN-550 was 25.0 μmol·g^{-1}, and the CH_3OH and C_2H_5OH selectivity reached 51.4 and 46.1%, respectively. The TC yield on Cu_2O/PCN was low. From Figure 4b, evidently, C_2H_5OH increased except for CH_3OH. Cu_2O/PCN without calcination promoted generat-

https://doi.org/10.1021/acsomega.2c01827
ACS Omega 2022, 7, 16817−16826

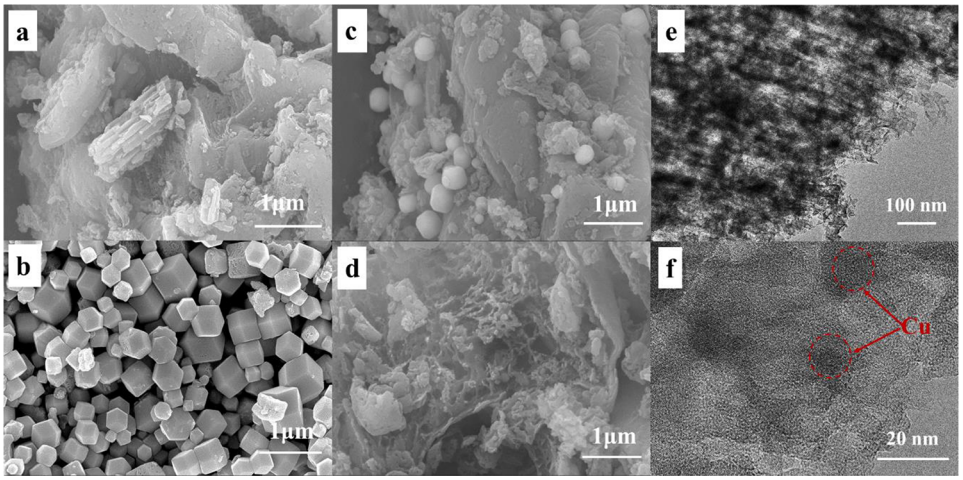

Figure 6. SEM images for (a) PCN, (b) Cu_2O, (c) Cu_2O/PCN-0.5, and (d) Cu/PCN-0.5. (e,f) HRTEM images for Cu/PCN-0.5.

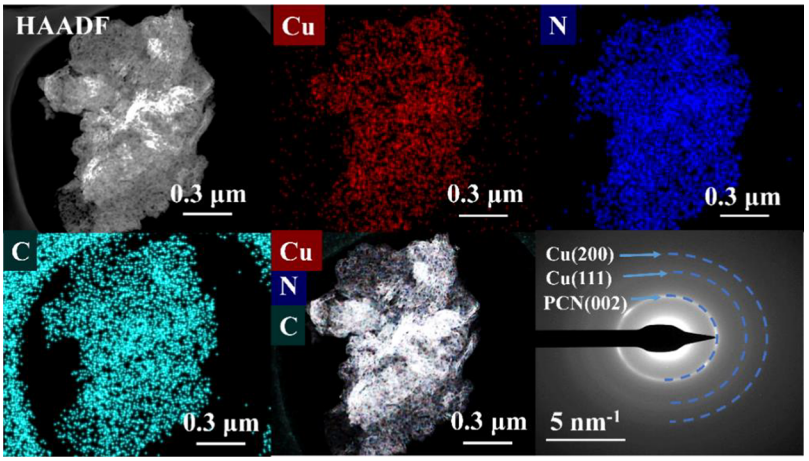

Figure 7. HAADF images, Cu, N, and C mapping, and SAED of Cu/PCN-0.5.

ing CH_3OH[16] and a small amount of C_2H_5OH. This strongly suggested that improvement in photoreaction activity mainly contributes to the formation of Cu. In addition, the CO and CH_4 yields exhibited a relatively small change, whereas the H_2 yield was higher when the calcination temperature was greater than 300 °C (Figure 4c,d). These results demonstrated that thermal reduction is indispensable for the activity of Cu/PCN toward the photogeneration of CH_3OH and C_2H_5OH. The production of H_2 indicated that H_2O oxidation simultaneously occurs, accompanying the reduction of CO_2.

Using different irradiation reaction times, the photoreaction activity of CO_2-aerated H_2O on Cu/PCN-0.5 was tested. From Figure 5a, as irradiation time extended from 0.5 to 8 h in separate runs, when the time was within 4 h, the CH_3OH and C_2H_5OH yields were higher. When the time exceeded 6 h, the yields became low, and the activity test for the 6 or 8 h reaction was repeated three times. The selectivity of CH_3OH + C_2H_5OH was greater than 85.7%. By contrast, from Figure 5b, as irradiation time extended, the CO and CH_4 yields showed a slight increase, and the H_2 yield displayed an evident increase. When the generated amounts of the products were depicted based on per hour (Figure S3), the CH_3OH and C_2H_5OH yields showed a certain decrease after 4 h irradiation reaction, whereas the CO, CH_4, and H_2 yields remained relatively stable. This may result from second reactions of CH_3OH and C_2H_5OH, for instance, the reverse oxidation induced by high light intensity[25] or the effect of undesorbed products on active sites.[27] Although after a 4 h irradiation reaction, the X-ray diffraction peaks of PCN remained unchanged, and the peaks of neither Cu nor copper oxides were observed, suggesting the structural stability of Cu/PCN-0.5 (Figure S4). However, a slight oxidation of Cu is not excluded during the photoreaction.

On the whole, this constructed Cu/PCN of a m-s heterojunction exhibited a higher photoreaction activity toward generation of CH_3OH and C_2H_5OH from CO_2-aerated H_2O, as compared with g-C_3N_4-based materials for photoreduction of CO_2 (Table S2).

Morphology and Dispersion. PCN from the protonation and exfoliation of g-C_3N_4 showed the layer-stacking structure (Figure 6a). Synthetic Cu_2O exhibited a uniform rhombic dodecahedral structure with even dispersion and no aggregation (Figure 6b). From Cu_2O/PCN-0.5 before thermal reduction (Figure 6c), Cu_2O monospherical particles were dispersed on the PCN surface. For Cu/PCN-0.5 undergoing calcination at 550 °C, the PCN surface was further exfoliated into porous layers due to thermal circumstances (Figure 6d). Meanwhile, the dispersed Cu_2O particles were reduced to Cu spreading into PCN layers. The above structure of Cu nanoparticles (NPs) on the porous layered surface of PCN were further observed (Figure 6e,f), demonstrating the formation of the Cu/PCN m-s heterojunction.

https://doi.org/10.1021/acsomega.2c01827
ACS Omega 2022, 7, 16817−16826

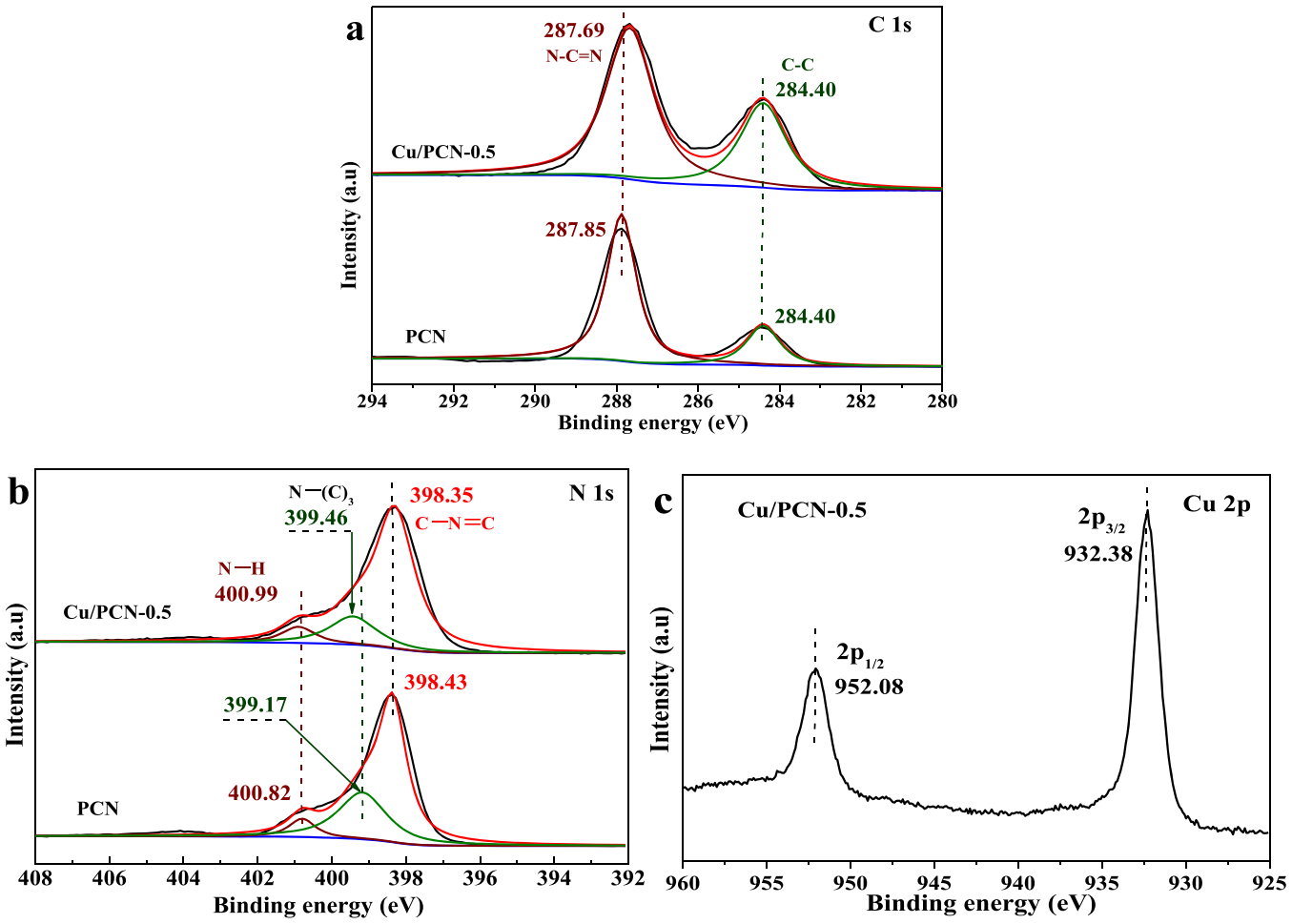

Figure 8. Comparison of (a) C 1s, (b) N 1s XPS spectra for PCN and Cu/PCN-0.5, and (c) Cu 2p high-resolution XPS of Cu/PCN-0.5.

A high-angle annular dark-field (HAADF) image (Figure 7) demonstrated the sparse and porous surface of Cu/PCN-0.5. Mapping results revealed the uniform distribution of Cu, N, and C elements in Cu/PCN-0.5. In addition, the selected area electron diffraction (SAED) rings of Cu(111), Cu(200), and PCN(002)[28] proved the existence of Cu crystals, which was not observed in the XRD phase analysis.

Synthesized samples showed type IV N_2 adsorption−desorption isotherms (Figure S5). The adsorption volume increased from $P/P_0 > 0.8$ due to the capillary coalescence. The H3-type hysteresis loop indicated the irregular fractured pore. Cu/PCN-0.5 showed higher specific surface area and pore volume than PCN due to a larger hysteresis loop and adsorption volume. Moreover, Cu/PCN-0.5 had more 5−50 nm mesopores than PCN. The increase in the specific surface area/pore volume and even dispersion of Cu on the PCN surface (Figures 6 and 7) promote the CO_2 adsorption and multielectron photoreactions for generation of CH_3OH and C_2H_5OH.

The surface elemental composition and valence state were analyzed using XPS. In the full spectrum (Figure S6), the electron binding energy peaks of Cu 2p, N 1s, and C 1s were observed. As shown in Figure 8a, the binding energies of 287.85 and 284.4 eV are attributed to the C atoms in N−C═N and surface C−C, respectively, whereas those of 400.82, 399.17, and 398.43 eV are attributed to the bridging N atoms in N−H, N−$(C)_3$, and C═N−C in PCN, respectively (Figure 8b). The shift of N 1s and C 1s by Cu/PCN-0.5 proved a strong interaction between Cu and the PCN surface.[29] Additionally, the binding energies of 952.08 and 932.38 eV in the spectra are ascribed to Cu 2p1/2 and Cu 2p3/2 of Cu^0, respectively (Figure 8c).[19]

Photoelectric Properties. Photoluminescence (PL) spectroscopy is one of effective methods to estimate the recombination rate of photogenerated carriers. A lower PL intensity implies longer lifetime of photogenerated electrons−holes, favorable for photocatalytic reactions. From Figure 9a, Cu/PCN-0.5 presented similar PL spectra with PCN. Its PL intensity, however, was far lower than that of PCN, which showed a broad absorption peak near 472 nm. The substantial decrease in the peak intensity indicated that recombination of carriers was greatly suppressed. The Cu/PCN m-s heterojunction possesses performances for rapid migration of photogenerated electrons and for retarding the charge recombination.[30]

From the PL spectra of Cu/PCN-*x* (Figure S2), Cu/PCN-1.5 showed the strongest peak, whereas Cu/PCN-0.1 had the weakest one, suggesting the difference of photogenerated electron−hole recombination rate on Cu/PCN with varied Cu amount. This proved that Cu can effectively capture the photogenerated electrons on PCN and promote the charge separation. However, Cu/PCN-0.5 exhibited the best photocatalytic activity, implying that PL is not the absolute indicator for catalytic performance. The PL decay properties of PCN

https://doi.org/10.1021/acsomega.2c01827
ACS Omega 2022, 7, 16817−16826

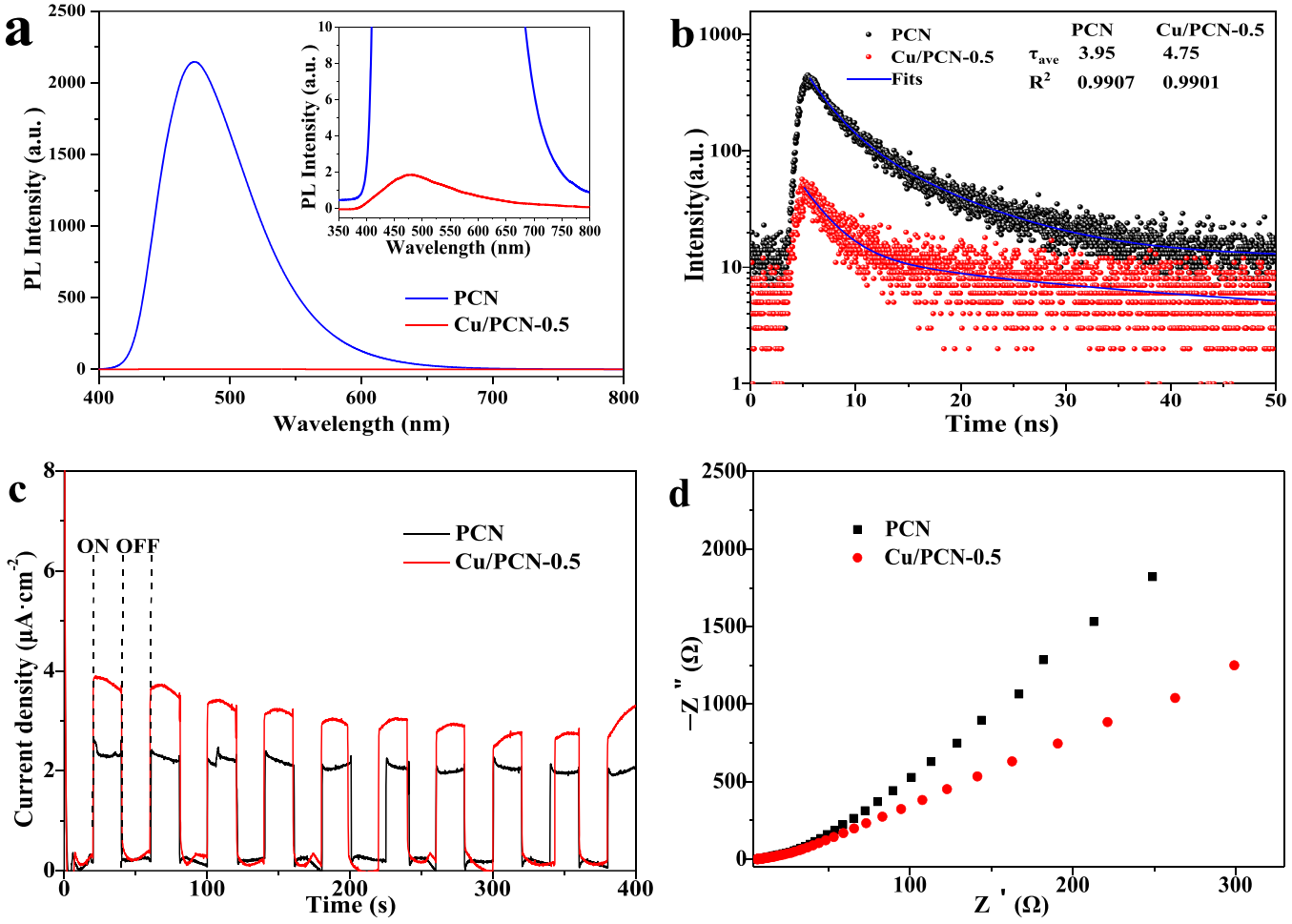

Figure 9. (a) PL spectra (inset for enlarged the *y* axis), (b) time-resolved PL spectra, (c) photocurrent response curves, and (d) Nyquist plots of PCN and Cu/PCN-0.5.

with Cu introduction were further revealed using time-resolved photoluminescence (TRPL) spectra. The Origin ExpDec2 basic function ($y = y_0 + A_1e^{(-x/\tau 1)} + A_2e^{(-x/\tau 2)}$) was employed to fit the average decay life ($\tau_{ave} = (A_1\tau_1^2 + A_2\tau_2^2)/(A_1\tau_1 + A_2\tau_2)$) with fit convergence matching $R^2 \geq 0.99$. From Figure 9b, the PL average lifetime of Cu/PCN-0.5 increased to 4.75 from 3.95 ns of PCN. A longer electron−hole lifetime favors the effective charge separation.[31] This can be attributed to the even dispersion of Cu on the PCN surface, which effectively extracts photogenerated electrons. As a result, the Cu/PCN m-s heterojunction interface improves the activity of photocatalytic reduction of CO_2 in H_2O. Cu/PCN-0.5 exhibits a CH_3OH yield of 12.85 μmol·g^{-1} during 4 h irradiation and was 2.47 times that of PCN (5.19 μmol·g^{-1}) (Figure 3). Although this change in the TRPL decay time in the interface is only a few nanoseconds, it affects the photoreaction activity significantly.

A stronger photocurrent represents better separation and transfer of photogenerated electrons and holes. The multiple cycle tests were carried out through the on/off switch of a lamp. As indicated in Figure 9c, the photocurrent signal was detected for PCN and Cu/PCN-0.5 under irradiation. The enhanced photocurrent density signal of Cu/PCN-0.5 can be attributed to higher electron extraction efficiency of Cu on the Cu-PCN interface, which accelerates the transport of photogenerated electrons and promotes the CO_2 reduction reaction. The semicircle radius of electrochemical impedance spectroscopy relates to the impedance. A smaller radius indicates lower resistance for the charge transfer. In Figure 9d, as the impedance semicircle radius of Cu/PCN-0.5 in the Nyquist curve became smaller, the charge transfer resistance in the interface region is lower. As a result, the Cu NPs on PCN as an electron reservoir lower the charge transfer resistance and provide more electrons for multielectron reduction reaction.

From the UV−vis diffuse reflectance absorption spectra (Figure S7), PCN with an absorption edge at 470 nm showed the UV and partially visible absorption range. The visible absorption properties of Cu/PCN-*x* were significantly improved. The visible absorption intensity increased with the Cu amount, and the sample color became gradually darker (Figure S6, inset). The absorption peak at 760 nm, ascribed to the Schottky effect, indicated the formation of the m-s heterojunction between Cu and PCN. The Mott−Schottky heterojunction interface can accelerate charge transfer, improving the catalytic activity.[32] The calculated band gaps of PCN and Cu/PCN-0.5 were 2.71 and 2.11 eV, respectively, using the Tauc equation, $(\alpha h\gamma)^{1/n} = A(h\nu - E_g)$ (Figure S8). As shown in Figure S9, the valence band (VB) positions were measured by the XPS valence band spectra. The VB positions of PCN and Cu/PCN-0.5 were 1.78 and 0.58 eV, respectively, whereas their conduction band (CB) positions were −0.99 and −1.53 eV, calculated from $E_g = E_{VB} - E_{CB}$, which matched the

https://doi.org/10.1021/acsomega.2c01827
ACS Omega 2022, 7, 16817−16826

reaction potentials of $E^{\theta}_{CO_2/CH_3OH}$ (−0.38 V), $E^{\theta}_{CO_2/C_2H_5OH}$ (−0.33 V), and $E^{\theta}_{H_2O/H_2}$ (−0.41 V).[9] As a result, more photoexcited electrons are beneficial to the 6*e*/12*e* reactions for CH_3OH/C_2H_5OH.

MECHANISM

The kinetics process of CO_2 photoreduction includes generation of carriers, transfer separation of electrons, and adsorption activation of CO_2/H_2O. The e^- and h^+ are involved in the redox reactions to produce CH_3OH, CO, CH_4, H_2, and O_2.[33] PCN is conducive to transport carriers for enhanced CO_2 reduction,[25,34] whereas metals on the semiconductor surface facilitate separation of carriers.[35]

The photoreaction pathway was proposed on the basis of the Schottky barrier mechanism on the cocatalyst metal−semiconductor interface and the characterization results. As shown in Figure 10, the well-dispersed Cu NPs on the PCN surface

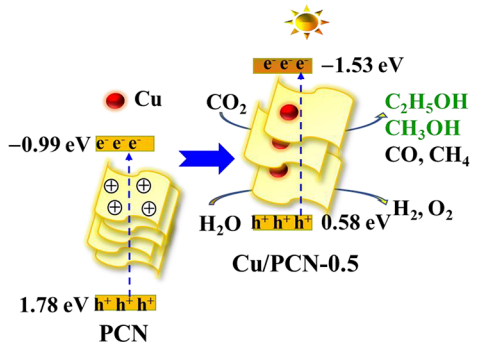

Figure 10. Electron transfer on Cu/PCN interface (pH of the reaction solution was ∼7, near pH 7 for NHE).

form the Cu-PCN m-s heterojunction. Under irradiation, electrons transit from the VB to the CB of PCN, and some of the photogenerated electrons are further transferred through the Schottky barrier from the CB of PCN to the Cu NPs' surface. The h^+ left on PCN first oxidizes H_2O to •OH and H^+. •OH, e^-, and h^+ are the active species,[36] which are indispensible for the photoreaction of CO_2 and H_2O on Cu/PCN-0.5, as confirmed by the active species capture experiments (Figure S10). Further activation of the intermediates and the formation of C−C coupling can be via the carbene (*CO) or formaldehyde (*HOCO) mechanisms as observed by in situ characterization.[37,38] The h^+ and e^- participate in the subsequent reactions for alcohol product formation.

The aforementioned photocurrent response curves, EIS, and PL spectra confirm the separation, transfer of carriers and suppression of their recombination on Cu/PCN. Change in the TRPL decay time proves the dynamic behavior of the charge carriers.[39] CO_2-aerated H_2O solution contains HCO_3^-, CO_3^{2-}, and H_2CO_3 reactive species (when the pH is about 7),[33] which is conducive to the product formation via the multielectron reactions involving e^- and h^+. Additionally, the VB position (0.58 eV) and the CB position (−1.53 eV) of Cu/PCN-0.5 match the redox potentials of CO_2-aerated H_2O and have more electrons for the redox reactions.[13,40,41]

CONCLUSIONS

A well-dispersed Cu/PCN m-s heterojunction was synthesized using thermal reduction with Cu_2O as the precursor for CO_2 to alcohols. In situ XRD validated the process from Cu_2O to Cu, and XPS confirmed a strong interaction between Cu and PCN. The Cu-PCN m-s heterojunction accelerated carrier migration, resulting in higher photocurrent density compared with that of PCN. The conduction band position (−1.53 eV) of Cu-PCN-0.5 was more negative and matched $E^{\theta}_{CO_2/CH_3OH}$ (−0.38 V) and $E^{\theta}_{CO_2/C_2H_5OH}$ (−0.33 V), providing more electrons for photoreaction of CO_2 and H_2O to CH_3OH and C_2H_5OH. Cu/PCN-0.5 exhibited a total carbon yield of 25.0 $\mu mol \cdot g^{-1}$ in 4 h irradiation reaction, which was 4.18 and 1.84 times that of PCN and Cu_2O/PCN, respectively. The selectivity for CH_3OH and C_2H_5OH was 51.42 and 46.14%, respectively. This work provides a new clue for Cu-PCN preparation and its application in generating alcohols from CO_2 reduction in H_2O.

EXPERIMENTAL SECTION

Materials. Melamine (99%), HNO_3 (65%), oleic acid (85−95%), $Cu(NO_3)_2 \cdot 3H_2O$ (99%), NaOH, and cyclohexane (99.5%) were purchased from Macklin Co. and used without further treatment. Deionized water was used for all experiments.

Catalyst Preparation. g-C_3N_4 was obtained through thermal polymerization. An appropriate amount of melamine powder in a corundum crucible was calcined at 550 °C for 4 h in a muffle furnace. After being cooled, the residue was ground in a marble mortar and yellow powder of g-C_3N_4 was obtained.

Protonated g-C_3N_4 was protonated and exfoliated. g-C_3N_4 and aqueous nitric acid solution (0.1 mol/L) were mixed in a ratio of 1:50 (g/mL), stirred vigorously for 2 h, sonicated for 2 h, stirred for another 2 h, centrifuged at 7000 rpm for 5 min, washed with deionized water and ethanol, and dried at 80 °C overnight to obtain the light-yellow powder of PCN.

To obtain Cu_2O, 40 mL of an aqueous solution of copper nitrate (0.025 mol/L) was placed in a three-necked flask with oil bath heating. Twenty-four milliliters of alcohol solution of oleic acid (oleic acid/ethanol: 1/5) was added and stirred vigorously for 0.5 h. Next, 8 mL of NaOH solution (1 mol/L) and 30 mL of glucose solution (0.02 mol/L) were dropped into the flask and stirred for 1 h to form an orange-red solution followed by centrifugation, washing using deionized water, cyclohexane, and ethanol, and then vacuum-dried at 80 °C overnight to obtain Cu_2O as a brick-red powder.

To obtain Cu/PCN-*x*, 0.1, 0.2, 0.5, 0.7, 1.0, or 1.5 g of PCN was added to 40 mL of $Cu(NO_3)_2$ solution (0.001 mol/L), and the same procedure as the Cu_2O preparation was used to obtain Cu_2O/PCN powder followed by calcination in a N_2 flow (20 mL/min) at 550 °C for 4 h and denoted as Cu/PCN-0.1, Cu/PCN-0.2, Cu/PCN-0.5, Cu/PCN-0.7, Cu/PCN-1.0, and Cu/PCN-1.5, respectively. The Cu amount in Cu/PCN is shown in Table S1. The Cu/PCN-0.5 sample calcined at 150, 300, or 550 °C for 4 h is denoted as Cu/PCN-150, Cu/PCN-300, or Cu/PCN-550, respectively.

Characterization. X-ray diffraction was conducted on a Rigaku XRD D8 with Cu Kα at 40 kV/40 mA. In situ XRD was carried out on Rigaku Smart Lab. A 50 mg sample was loaded into an in situ cell. In a N_2 flow (10 mL/min) of normal pressure, as the sample was heated from 25 to 550 °C at 10 °C/min, the XRD pattern was recorded at an interval of 50 °C for 30 min hold and an interval of 30 min at 550 °C for 4 h. The specific surface area was calculated by means of N_2 adsorption on a JW-BK132F instrument. Microscopic morphology was observed on a scanning electron microscope (Zeiss Merlin Compact/Oxford x-max) at 520 kV using the

https://doi.org/10.1021/acsomega.2c01827
ACS Omega 2022, 7, 16817−16826

gold-sprayed sample and on a field emission transmission electron microscope (FEI Talos F200i). The surface composition of the sample was analyzed on a Thermo Scientific K-Alpha X-ray photoelectron spectrometer, Al Kα, with C 1s (284.6 eV) as the background correction.

The photoluminescence spectra were measured on an Edinburgh FLS1000 steady-state/transient fluorescence spectrometer at an excitation wavelength of 325 nm. The diffuse reflectance spectra were measured on a Shimadzu UV-3600 UV−vis−NIR spectrophotometer. The band gap energy (E_g) was calculated according to the Kubelka−Munk equation $(\alpha h\nu)^{1/n} = A(h\nu - E_g)$, where α is the absorption coefficient and n is 1/2 or 2. Specifically, E_g was obtained from the intersection of the starting curve with the $h\nu$ axis.[42] The transient photocurrent response and photochemical impedance were measured at a CHI 760E electrochemical workstation. For working electrode preparation, a 3 mg sample was placed in a centrifuge tube. Then 200 μL of ethanol and 10 μL of 0.5% Nafen solution were added and ultrasonically dispersed for 1 h. Ag/AgCl, Pt electrode, and Na_2SO_4 (0.5 mol/L) were used as reference, counter electrodes, and electrolyte solution, respectively.

Photoreaction Activity Test. The photoreaction of CO_2 with H_2O was conducted in a photoreactor with a 100 mL internal volume, with a quartz window on top and a 300 W UV−vis xenon lamp light source of luminous power of 2.5 W (Figure S10). Forty milligrams of a catalyst sample and 40 mL of aqueous solution containing NaOH (0.1 mol/L) and Na_2SO_3 (0.1 mol/L) were placed in the reactor followed by evacuation and CO_2 replacement three times. Then CO_2 (20 mL/min) was switched for 0.5 h and increased to 0.2 MPa. The reaction started at the set conditions. After the reaction, the gaseous sample was analyzed on a gas chromatograph (GC9560) TCD with a 5 A molecular sieve column (3m × 3 mm) for H_2, O_2, CO, and CH_4 separation. The liquid sample was collected with a 0.45 μm filter and analyzed on another GC9560 FID with a FFAP column (30 m × 0.25 mm × 0.25 μm) for oxygenate separation. Results were calculated as yield (Y_i, μmol·g^{-1}) = n_i/m, where n_i is the product amount (μmol) and m is the mass of entire catalyst (g); the total carbon (TC) yield (μmol·g^{-1}) = $Y_{CO} + Y_{CH_4} + Y_{CH_3OH} + Y_{C_2H_5OH}$; product selectivity (Si, %) = (Y_i/TC) × 100. To identify the carbon origin for the products, contrast experiments of the activity test were performed, and the results are shown in Table S3. When H_2O, irradiation, CO_2, or Cu/PCN-0.5 was not employed, no products were detected (entries 2−5), indirectly indicating that the carbons in the products come from CO_2 under the light irradiation conditions rather than from the Cu/PCN-0.5 catalyst. To understand the reactive species in the reaction process, the active species capture experiments on Cu/PCN-0.5 were carried out under the same reaction conditions.

■ ASSOCIATED CONTENT

Supporting Information

The Supporting Information is available free of charge at https://pubs.acs.org/doi/10.1021/acsomega.2c01827.

Photoreactor; contrast experiments for carbon origin; activity comparison of g-C_3N_4-containing catalysts for CO_2 reduction; experimental details for Cu/PCN including XRD, pore distribution, PL spectra, diffuse reflectance UV−vis spectra, and XPS (PDF)

■ AUTHOR INFORMATION

Corresponding Author

Tian-Sheng Zhao − *State Key Laboratory of High-efficiency Utilization of Coal and Green Chemical Engineering, College of Chemistry & Chemical Engineering, Ningxia University, Yinchuan 750021, China;* orcid.org/0000-0002-2292-3194; Email: zhaots@nxu.edu.cn

Authors

Huihui Du − *State Key Laboratory of High-efficiency Utilization of Coal and Green Chemical Engineering, College of Chemistry & Chemical Engineering, Ningxia University, Yinchuan 750021, China*

Xinhua Gao − *State Key Laboratory of High-efficiency Utilization of Coal and Green Chemical Engineering, College of Chemistry & Chemical Engineering, Ningxia University, Yinchuan 750021, China;* orcid.org/0000-0003-1368-1901

Qingxiang Ma − *State Key Laboratory of High-efficiency Utilization of Coal and Green Chemical Engineering, College of Chemistry & Chemical Engineering, Ningxia University, Yinchuan 750021, China*

Xiaojiao Yang − *State Key Laboratory of High-efficiency Utilization of Coal and Green Chemical Engineering, College of Chemistry & Chemical Engineering, Ningxia University, Yinchuan 750021, China*

Complete contact information is available at: https://pubs.acs.org/10.1021/acsomega.2c01827

Notes

The authors declare no competing financial interest.

■ ACKNOWLEDGMENTS

The authors acknowledge financial support from the National Natural Science Fund of China (21965028) and the East-West cooperation project of Ningxia Key R&D Plan (2017BY063).

■ REFERENCES

(1) Zhu, S.; Chen, X.; Li, Z.; Ye, X.; Liu, Y.; Chen, Y.; Yang, L.; Chen, M.; Zhang, D.; Li, G.; Li, H. Cooperation between inside and outside of TiO_2: Lattice Cu^+ accelerates carrier migration to the surface of metal copper for photocatalytic CO_2 reduction. *Appl. Catal. B: Environ.* **2020**, *264*, 118515.

(2) Zhu, Z.; Chen, C.-Y.; Wu, R.-J. Hydrocarbon production by addition of Cu-ZnO on g-C_3N_4 for CO_2 conversion. *J. Chin. Chem. Soc-Taip.* **2020**, *67* (9), 1654−1660.

(3) Zhu, Z.; Yang, C.-X.; Hwang, Y.-T.; Lin, Y.-C.; Wu, R.-J. Fuel generation through photoreduction of CO_2 on novel Cu/$BiVO_4$. *Mater. Res. Bull.* **2020**, *130*, 110955.

(4) Tahir, M. Hierarchical 3D VO_2/ZnV_2O_4 microspheres as an excellent visible light photocatalyst for CO_2 reduction to solar fuels. *Appl. Surf. Sci.* **2019**, *467*, 1170−1180.

(5) Zhang, Q.; Yin, J.-Y.; Tian, Z.-Y.; Xu, W.-C.; Yang, N.; Yao, S.; Zhang, Z.-M. Construction of C_3N_4/$BiVO_4$/Cu_2O composite for CO_2 photoreduction to methanol in pure water. *Int. J. Mol. Sci.* **2021**, *37* (4), 335−342.

(6) Liu, S.-H.; Lu, J.-S.; Pu, Y.-C.; Fan, H.-C. Enhanced photoreduction of CO_2 into methanol by facet-dependent Cu_2O/reduce graphene oxide. *J. CO2. Util.* **2019**, *33*, 171−178.

(7) Cao, S.; Low, J.; Yu, J.; Jaroniec, M. Polymeric photocatalysts based on graphitic carbon nitride. *Adv. Mater.* **2015**, *27* (13), 2150−2176.

(8) Ren, Y.; Zeng, D.; Ong, W.-J. Interfacial engineering of graphitic carbon nitride (g-C_3N_4)-based metal sulfide heterojunction photo-

catalysts for energy conversion: A review. *Chin. J. Catal.* **2019**, *40* (3), 289−319.
(9) Ong, W.-J.; Tan, L.-L.; Ng, Y. H.; Yong, S.-T.; Chai, S.-P. Graphitic Carbon Nitride ($g\text{-}C_3N_4$)-Based Photocatalysts for Artificial Photosynthesis and Environmental Remediation: Are We a Step Closer To Achieving Sustainability? *Chem. Rev.* **2016**, *116* (12), 7159−7329.
(10) Di, Y.; Wang, X.; Thomas, A.; Antonietti, M. Making Metal-Carbon Nitride Heterojunctions for Improved Photocatalytic Hydrogen Evolution with Visible Light. *ChemCatChem.* **2010**, *2* (7), 834−838.
(11) Han, T.; Xie, C. M.; Meng, Y. J.; Wei, Y. Synthesized MnO_2/Ag/$g\text{-}C_3N_4$ composite for photoreduction carbon dioxide under visible light. *J. Mater. Sc-Mater. El.* **2018**, *29* (24), 20984−20990.
(12) Cao, S.; Li, Y.; Zhu, B.; Jaroniec, M.; Yu, J. Facet effect of Pd cocatalyst on photocatalytic CO_2 reduction over $g\text{-}C_3N_4$. *J. Catal.* **2017**, *349*, 208−217.
(13) Ali, S.; Razzaq, A.; Kim, H.; In, S.-I. Activity, selectivity, and stability of earth-abundant $CuO/Cu_2O/Cu^0$-based photocatalysts toward CO_2 reduction. *Chem. Eng. J.* **2022**, *429*, 131579.
(14) Yuan, X.; Chen, S.; Cheng, D.; Li, L.; Zhu, W.; Zhong, D.; Zhao, Z.-J.; Li, J.; Wang, T.; Gong, J. Controllable Cu^0-Cu^+ Sites for Electrocatalytic Reduction of Carbon Dioxide. *Angew. Chem. Int. Ed.* **2021**, *60* (28), 15344−15347.
(15) Chang, P.-Y.; Tseng, I.-H. Photocatalytic conversion of gas phase carbon dioxide by graphitic carbon nitride decorated with cuprous oxide with various morphologies. *J. CO2 Util.* **2018**, *26*, 511−521.
(16) Tian, Z. Y.; Kong, L. H.; Wang, Y.; Wang, H.-J.; Wang, Y.-J.; Yao, S.; Lu, T.-B.; Zhang, Z.-M. Construction of Low-Cost Z-Scheme Heterostructure Cu_2O/PCN for Highly Selective CO_2 Photoreduction to Methanol with Water Oxidation. *Small* **2021**, *17* (44), 2103558.
(17) Zhao, X.; Fan, Y.; Zhang, W.; Zhang, X.; Han, D.; Niu, L.; Ivaska, A. Nanoengineering Construction of Cu_2O Nanowire Arrays Encapsulated with $g\text{-}C_3N_4$ as 3D Spatial Reticulation All-Solid-State Direct Z-Scheme Photocatalysts for Photocatalytic Reduction of Carbon Dioxide. *ACS Catal.* **2020**, *10* (11), 6367−6376.
(18) Wu, Y. A.; McNulty, I.; Liu, C.; Lau, K. C.; Liu, Q.; Paulikas, A. P.; Sun, C.-J.; Cai, Z.; Guest, J. R.; Ren, Y.; Stamenkovic, V.; Curtiss, L. A.; Liu, Y.; Rajh, T. Facet-dependent active sites of a single Cu_2O particle photocatalyst for CO_2 reduction to methanol. *Nat. Energy* **2019**, *4* (11), 957−968.
(19) Li, P.; Liu, L.; An, W.; Wang, H.; Guo, H.; Liang, Y.; Cui, W. Ultrathin porous $g\text{-}C_3N_4$ nanosheets modified with AuCu alloy nanoparticles and C-C coupling photothermal catalytic reduction of CO to ethanol. *Appl. Catal. B: Environ.* **2020**, *266*, 118618.
(20) Fan, Q.; Zhang, X.; Ge, X.; Bai, L.; He, D.; Qu, Y.; Kong, C.; Bi, J.; Ding, D.; Cao, Y.; Duan, X.; Wang, J.; Yang, J.; Wu, Y. Manipulating Cu Nanoparticle Surface Oxidation States Tunes Catalytic Selectivity toward CH_4 or C_2^+ Products in CO_2 Electroreduction. *Adv. Energy Mater.* **2021**, *11* (36), 2101424.
(21) Zhao, J.; Xue, S.; Barber, J.; Zhou, Y.; Meng, J.; Ke, X. An overview of Cu-based heterogeneous electrocatalysts for CO_2 reduction. *J. Mater. Chem. A* **2020**, *8* (9), 4700−4734.
(22) Jiang, Z.; Sun, W.; Miao, W.; Yuan, Z.; Yang, G.; Kong, F.; Yan, T.; Chen, J.; Huang, B.; An, C.; Ozin, G. A. Living Atomically Dispersed Cu Ultrathin TiO_2 Nanosheet CO_2 Reduction Photocatalyst. *Adv. Sci.* **2019**, *6* (15), 1900289.
(23) Sayed, M.; Zhang, L.; Yu, J. Plasmon-induced interfacial charge-transfer transition prompts enhanced CO_2 photoreduction over Cu/Cu_2O octahedrons. *Chem. Eng. J.* **2020**, *397*, 125390.
(24) Liu, Y. X.; Wang, H. H.; Zhao, T.-J.; Zhang, B.; Su, H.; Xue, Z.-H.; Li, X.-H.; Chen, J.-S. Schottky Barrier Induced Coupled Interface of Electron-Rich N-Doped Carbon and Electron-Deficient Cu: In-Built Lewis Acid-Base Pairs for Highly Efficient CO_2 Fixation. *J. Am. Chem. Soc.* **2019**, *141* (1), 38−41.
(25) Tahir, M.; Tahir, B.; Nawawi, M. G. M.; Hussain, M.; Muhammad, A. Cu-NPs embedded 1D/2D CNTs/pCN heterojunction composite towards enhanced and continuous photocatalytic CO_2 reduction to fuels. *Appl. Surf. Sci.* **2019**, *485*, 450−461.
(26) Qin, Y.; Dong, G.; Zhang, L.; Li, G.; An, T. Highly efficient and selective photoreduction of CO_2 to CO with nanosheet $g\text{-}C_3N_4$ as compared with its bulk counterpart. *Environ. res.* **2021**, *195*, 110880.
(27) Albo, J.; Garcia, G. Enhanced visible-light photoreduction of CO_2 to methanol over Mo_2C/TiO_2 surfaces in an optofluidic microreactor. *React. Chem. Eng.* **2021**, *6* (2), 304−312.
(28) Xu, J.; Wu, F.; Jiang, Q.; Li, Y.-X. Mesoporous carbon nitride grafted with n-bromobutane: a high-performance heterogeneous catalyst for the solvent-free cycloaddition of CO_2 to propylene carbonate. *Catal. Sci. Technol.* **2015**, *5* (1), 447−454.
(29) Li, C.; Yu, S.; Dong, H.; Wang, Y.; Wu, H.; Zhang, X.; Chen, G.; Liu, C. Mesoporous ferriferous oxide nanoreactors modified on graphitic carbon nitride towards improvement of physical, photoelectrochemical properties and photocatalytic performance. *J. Colloid Interface Sci.* **2018**, *531*, 331−342.
(30) Sun, Z.; Fang, W.; Zhao, L.; Chen, H.; He, X.; Li, W.; Tian, P.; Huang, Z. $g\text{-}C_3N_4$ foam/Cu_2O QDs with excellent CO_2 adsorption and synergistic catalytic effect for photocatalytic CO_2 reduction. *Environ. Int.* **2019**, *130*, 104898.
(31) Li, A.; Wang, T.; Li, C.; Huang, Z.; Luo, Z.; Gong, J. Adjustable Reduction Potential of Electrons via Quantum Confinement for Selective CO_2 Photoreduction to Methanol. *Angew. Chem. Int. Ed.* **2019**, *58* (12), 3804−3808.
(32) Li, X.-H.; Antonietti, M. Metal nanoparticles at mesoporous N-doped carbons and carbon nitrides: functional Mott-Schottky heterojunctions for catalysis. *Chem. Soc. Rev.* **2013**, *42* (16), 6593−6604.
(33) Li, X.; Yu, J.; Jaroniec, M.; Chen, X. Cocatalysts for Selective Photoreduction of CO_2 into Solar Fuels. *Chem. Rev.* **2019**, *119* (6), 3962−4179.
(34) Tahir, B.; Tahir, M.; Che Yunus, M. A.; Mohamed, A. R.; Siraj, M.; Fatehmulla, A. 2D/2D Mt/m-CN composite with enriched interface charge transfer for boosting photocatalytic CO_2 hydrogenation by H_2 to CH_4 under visible light. *Appl. Surf. Sci.* **2020**, *520*, 146296.
(35) Tahir, B.; Tahir, M.; Amin, N. A. S. Silver loaded protonated graphitic carbon nitride ($Ag/pg\text{-}C_3N_4$) nanosheets for stimulating CO_2 reduction to fuels via photocatalytic bi-reforming of methane. *Appl. Surf. Sci.* **2019**, *493*, 18−31.
(36) Wang, K.; Feng, X.; Shangguan, Y.; Wu, X.; Chen, H. Selective CO_2 photoreduction to CH_4 mediated by dimension-matched 2D/2D $Bi_3NbO_7/g\text{-}C_3N_4$ S-scheme heterojunction. *Chin. J. Catal.* **2022**, *43* (2), 246−254.
(37) Montoya, J. H.; Peterson, A. A.; Nørskov, J. K. Insights into C-C Coupling in CO_2 Electroreduction on Copper Electrodes. *ChemCatChem.* **2013**, *5* (3), 737−742.
(38) Kortlever, R.; Shen, J.; Schouten, K. J. P; Calle-Vallejo, F.; Koper, M. T. M. Catalysts and Reaction Pathways for the Electrochemical Reduction of Carbon Dioxide. *J. Phys. Chem. Lett.* **2015**, *6* (20), 4073−4082.
(39) Li, X.; Wen, J.; Low, J.; Fang, Y.; Yu, J. Design and fabrication of semiconductor photocatalyst for photocatalytic reduction of CO_2 to solar fuel. *Sci. China Mater.* **2014**, *57* (1), 70−100.
(40) Fu, J.; Zhu, B.; Jiang, C.; Cheng, B.; You, W.; Yu, J. Hierarchical Porous O-Doped $g\text{-}C_3N_4$ with Enhanced Photocatalytic CO_2 Reduction Activity. *Small* **2017**, *13* (15), 1603938.
(41) Tahir, B.; Tahir, M.; Mohd Nawawi, M. G. Well-Designed 3D/2D/2D WO_3/Bt/$g\text{-}C_3N_4$ Z-Scheme Heterojunction for Tailoring Photocatalytic CO_2 Methanation with 2D-Layered Bentonite-Clay as the Electron Moderator under Visible Light. *Energy Fuel.* **2020**, *34* (11), 14400−14418.
(42) Dedong, Z.; Maimaiti, H.; Awati, A.; Yisilamu, G.; Fengchang, S.; Ming, W. Synthesis and photocatalytic CO_2 reduction performance of Cu_2O/Coal-based carbon nanoparticle composites. *Chem. Phys. Lett.* **2018**, *700*, 27−35.

https://doi.org/10.1021/acsomega.2c01827
ACS Omega 2022, 7, 16817−16826